processes

MDPI

Article

3-D Modeling of Dehydration Kinetics and Shrinkage of Ellipsoidal Fermented Amazonian Cocoa Beans

Alessandra Adrover [1,2,*] and Antonio Brasiello [1,2]

[1] Dipartimento di Ingegneria Chimica, Materiali e Ambiente, Sapienza Università di Roma, Via Eudossiana 18, 00184 Rome, Italy

[2] INSTM Consorzio Interuniversitario Nazionale per la Scienza e Tecnologia dei Materiali, Via G. Giusti 9, 50121 Firenze, Italy; antonio.brasiello@uniroma1.it

* Correspondence: alessandra.adrover@uniroma1.it; Tel.: +39-06-44585608

Received: 30 December 2019; Accepted: 20 January 2020; Published: 24 January 2020

Abstract: A recently proposed moving-boundary model for food isothermal dehydration was applied to analyze the dehydration kinetics of ellipsoidal cocoa beans, characterized by a moderate shrinkage and a non-uniform initial distribution of water content between the core and the shell of the bean. The aim is to predict the influence of air velocity and non-uniformity of the initial water distribution on the dehydration rates, as well as the temporal evolution of the water content in the core and in the shell and of the characteristic lengths of the ellipsoidal bean. The model proved capable of accurately describing the two-phases dehydration process: an initial fast dehydration of the shell, characterized by higher dehydration rates, followed by a slower dehydration of the core, characterized by a linear relationship $j_d = \delta(T)X_r$ between the dehydration rate j_d and the moisture ratio X_r. A shortcut method to estimate the effective water diffusivity D is also proposed, deriving from the basic observation that the asymptotic exponential behaviour of the dehydration curve $X_r(t)$ for an ellipsoidal bean coincides with that of an equivalent sphere, with the same surface-to-volume ratio.

Keywords: drying kinetics; 3-d modeling; moving-boundary model; diffusion coefficient; cocoa beans

1. Introduction

The cocoa beans extracted from the fruit of the cocoa tree (*Theobroma cacao*, see Figure 1) are the raw material for chocolate production [1]. Cocoa beans are usually subjected to fermentation and drying [2–6]. The principal aim of drying is to reduce the moisture content, the main culprit of bean spoilage due to bacteria, yeast, and mould growth. The drying operation can be provided by two methods: natural drying [7], when cocoa beans are spread on a support and exposed directly to sun, or artificial convective drying [3], in which cocoa beans are placed in a dryer and exposed to an air flow with controlled velocity, temperature and humidity. The main drawbacks of natural drying are connected to weather unpredictability which could cause prolonged drying duration and products' spoilage whereas the advantages of artificial drying are paid with high energy and plant costs [5,6].

The cocoa fruit are usually ellipsoidal in shape and the internal structure consists of a central core surrounded by a thin shell [8], representing about 20% of the total mass of the bean [9,10]. The water content in the core and the shell can be very different and this may have a strong influence on the dehydration kinetics that is accompanied by a moderate volume reduction (shrinkage), about 30% of the initial volume.

Mathematical modeling of cocoa bean's drying kinetics can be a useful tool to identify the best operative conditions, in the case of artificial drying, or to estimate the optimal drying time, in the case of natural drying.

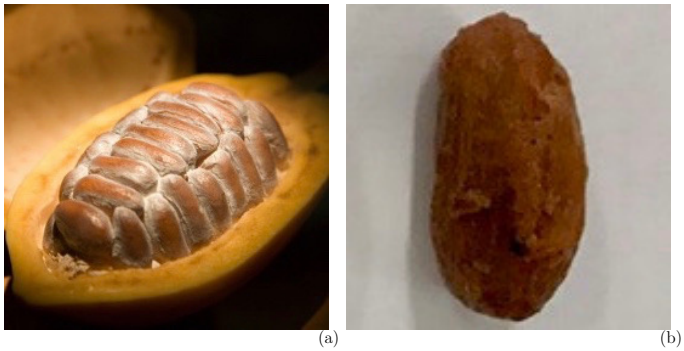

Figure 1. Cocoa fruit (**a**) and fermented Amazonian cocoa bean (**b**).

Few attempts were made, in the recent literature, to model the dehydration kinetics of cocoa beans in all its complexity related to the ellipsoidal shape of the bean (intrinsic 3-d problem [6,11]), to the volume shrinkage [12] and to the necessity to account for mass transfer resistance at the solid/air interface [6,11].

The general objective of this work is to apply the moving-boundary model for food isothermal dehydration, recently proposed by Adrover et al. [13,14], to analyze and characterize the dehydration kinetics and shrinkage of cocoa beans, starting from the experimental data reported by Herman et al. [9,10] who have recently published the results of an extensive experimental campaign on fermented Amazonian cocoa beans. In [9,10], Herman et al. investigate the temporal evolution, during convective drying, of the water content in the core and the shell of fermented Amazonian cocoa beans, in order to better characterize the drying kinetics and to investigate the influence of operating parameters, namely the air velocity and the drying temperature.

The moving-boundary model by Adrover et al. [13,14] was already successfully applied to describe the dehydration kinetics and shrinkage of different food materials and different sample shapes, e.g., eggplant cylindrical [14] and discoidal samples [15], chajote slices [16], potatoes sticks [14] and square slices [13].

In this work, the moving-boundary model is applied to 3-d ellipsoidal beans, accounting for the specific internal structure of the bean (core and shell), the non-uniformity of the initial water content and the volume shrinkage in order to better understand and to accurately describe the two-phases dehydration process of cocoa beans, as observed by Herman et al. [9,10]: an initial fast dehydration of the shell, characterized by higher dehydration rates, followed by a slower dehydration of the core, characterized by a linear relationship between the dehydration rate j_d and the moisture ratio X_r.

The article is organized as follows. In Section 2, a review of the morphological and physical parameters of fermented Amazonian cocoa beans is presented, thus highlighting the differences, in the initial distribution of the moisture content and in the final shrinkage, between two different sets of cocoa beans whose dehydration kinetics will be analyzed.

In Section 3, the basic equations for the isothermal moving-boundary model are presented and subsequently applied to ellipsoidal beans in order to investigate: (i) the influence of the ellipsoidal shape on dehydration kinetics in the simplest case of a uniform initial water distribution; (ii) the influence of a nonuniform initial water distribution on dehydration rates, in the absence of shrinkage; (iii) the influence, on dehydration rates, of a constant shrinkage factor.

Section 4 is devoted to modeling the dehydration kinetics and shrinkage of Amazonian cocoa beans, thus obtaining: (i) a reliable estimate of the effective water diffusivity at different temperatures; (ii) an accurate prediction of the influence of air velocity and non-uniformity of the initial water distribution on dehydration kinetics; (iii) a correct description of the temporal evolution of the moisture content and thickness of core and shell.

2. Morphological and Physical Characterization of Ellipsoidal Cocoa Beans

We analyze experimental data of hot-air drying of fermented Amazonian cocoa beans (data from Herman et al. [9,10]) in a convective dryer at different temperatures $T = 30, 40, 50, 60$ °C and different air velocities $v = 0.3, 0.6, 1$ m/s. Fermented Amazonian cocoa beans were fermented at 30 °C for seven days in wooden boxes and stored at -18 °C until drying. Two different sets of data are analyzed and compared. Data set (1) from [9] and data set (2) from [10] both refer to fermented Amazonian beans (*Theobroma cacao*, var. *Forasteiro*) from Quatro-Bocas, State of Pará, Brasil, with ellipsoidal shape (see Figure 2).

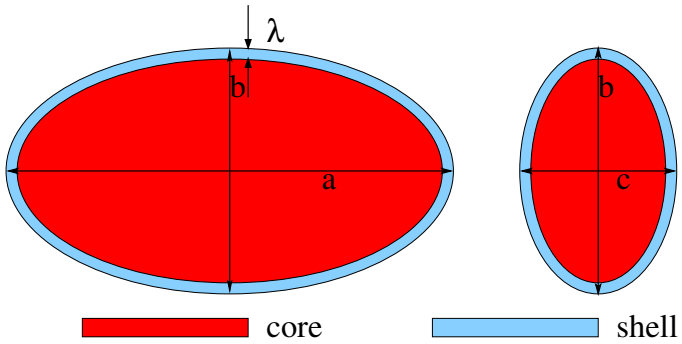

Figure 2. Scaled representation of an ellipsoidal cocoa bean (core and shell). a, b and c are the three principal axes and λ is the shell thickness.

The main morphological and physical parameters, namely the initial length of the three principal axes a_0, b_0, c_0, the initial shell thickness λ_0, the initial total moisture content X_0 and the initial moisture content of the core X_0^{core}, are reported in Table 1.

Table 1. Morphological and physical parameters of two different sets of freshly fermented Amazonian cocoa beans. Data set (1) are reported in [9]. Data set (2) are reported in [10].

Data Set	a_0 (mm)	b_0 (mm)	c_0 (mm)	λ_0 (mm)	X_0 (kg/kg db)	X_0^{core} (kg/kg db)	X_0^{core}/X_0 (-)	V_0^{core}/V_0 (-)
(1)	24.7 ± 0.72	12.73 ± 0.5	8.94 ± 0.86	0.45 ± 0.09	0.82 ± 0.09	0.6 ± 0.08	$\simeq 0.73$	$\simeq 0.8$
(2)	24.28 ± 1.57	13.34 ± 0.5	8.52 ± 0.35	0.58 ± 0.09	$\simeq 0.88$	$\simeq 0.49$	$\simeq 0.56$	$\simeq 0.72$

Specifically, the initial moisture content of the core X_0^{core} was experimentally evaluated by peeling the fresh shell and then drying separately the core and the shell for 24 h at 105 °C, thus evaluating X_0^{core} as

$$X_0^{core} = \frac{M_0^{core} - M_d^{core}}{M_d^{core} + M_d^{shell}} \tag{1}$$

where M_0^{core} is the mass of the fresh core, M_d^{core} and M_d^{shell} are the mass of the dry core and of the dry shell, respectively. For a detailed discussion about the experimental procedure see [9].

From the initial mass $M_0 \simeq 1.87 \pm 0.24$ g and the initial moisture content X_0, the initial volume fraction ϕ_0 (averaged over the entire bean, i.e., core and shell) of water inside the cocoa bean, before drying, can been estimated as follows

$$\phi_0 = \frac{M_0 - M_d}{\rho_w V_0} = \frac{M_0}{\rho_w V_0} \frac{X_0}{1 + X_0} \tag{2}$$

where $M_d = M_d^{core} + M_d^{shell}$ is the total dry mass and ρ_w is the water density, thus obtaining $\phi_0 \simeq 0.57$ for data set (1) and $\phi_0 = 0.59$ for data set (2).

The volume fraction of water in the core ϕ_0^{core} and in the shell ϕ_0^{shell} can been evaluated, from the material balance

$$\phi_0 V_0 = \phi_0^{core} V_0^{core} + \phi_0^{shell} V_0^{shell} \tag{3}$$

as follows

$$\phi_0^{core} = \phi_0 \underbrace{\frac{X_0^{core}/X_0}{V_0^{core}/V_0}}_{\beta_0^{core}}, \quad \phi_0^{shell} = \phi_0 \underbrace{\frac{1 - X_0^{core}/X_0}{1 - V_0^{core}/V_0}}_{\beta_0^{shell}} \tag{4}$$

From the morphological and physical parameters reported in Table 1, it can be observed that the two sets of cocoa beans differ significantly in the ratio X_0^{core}/X_0 and this implies very different values for the partition factors β_0^{core} and β_0^{shell}, namely $\beta_0^{core} \simeq 0.912$ and $\beta_0^{shell} \simeq 1.35$ for data set (1) and $\beta_0^{core} \simeq 0.78$ and $\beta_0^{shell} \simeq 1.53$ for data set (2). The higher the value of water concentration in the shell, the faster the decrease of the total moisture content at the beginning of the drying process, and therefore the larger the initial dehydration rate.

Focusing on volume shrinkage, the sample volume V_d after complete drying, can be estimated from data reported in [9,10]. In [9], Herman et al. evaluated the volume $V_0 = (\pi/6)a_0 b_0 c_0$ of the fresh bean as well as the volume of the dry bean $V_d = (\pi/6)a_d b_d c_d$, where a_d, b_d, c_d represent the lengths of the principal axes of the bean after drying. These authors approximate the ellipsoidal shape of the bean with a cylinder of height $H = a$ and radius $R = \sqrt{bc/6}$, i.e., a cylinder with the same volume as the ellipsoid and height H equal to the length a of the main principal axes of the ellipsoid. As a consequence, they report the morphological parameters of the fresh bean as $a_0 = 25.5$ mm, $R_0 = 4.5$ mm and the shrinkage parameters as $a_d/a_0 = 0.93 \pm 0.09$ and $R_d/R_0 = 0.94 \pm 0.019$, a_d and R_d being the height and the radius of the equivalent cylinder, after drying. From these data, it is possible to estimate the rescaled dry-sample volume V_d/V_0 as

$$\frac{V_d}{V_0} = \frac{\pi a_0 R_0^2}{\pi a_d R_d^2} = \left(\frac{a_d}{a_0}\right)\left(\frac{R_d}{R_0}\right)^2 \simeq 0.82 \tag{5}$$

The rescaled dry-sample volume $V_d/V_0 \simeq 0.82$ obtained from data set (1) [9] is in agreement with that obtained from data set (2) [10]. In [10], the authors report the three ratios $a_d/a_0 \simeq 0.88$, $b_d/b_0 \simeq 0.94$ and $c_d/c_0 \simeq 0.94$ for the principal axes of the ellipse, so that the rescaled dry-sample volume V_d/V_0 can be directly evaluated as

$$\frac{V_d}{V_0} = \left(\frac{a_d}{a_0}\right)\left(\frac{b_d}{b_0}\right)\left(\frac{c_d}{c_0}\right) \simeq 0.78 \tag{6}$$

This slightly larger shrinkage is reasonably due to the higher initial moisture content X_0.

These experimental findings are also in agreement with shrinkage data reported by Koua et al. [7] for indirect solar drying of cocoa beans from Cote d'Ivore. Ellipsoidal cocoa beans used by Koua et al. are bigger than Amazonian cocoa beans used by Herman et al. Indeed, the lengths of the three principal axes are $a_0 = 27.6$ mm, $b_0 = 15.5$ mm and $c_0 = 11.3$ mm and also the initial moisture content $X_0 = 1.22$ (kg/kg db) is larger than that for Amazonian cocoa beans. Koua et al. experimentally observed a linear relationship between the rescaled volume V/V_0 and the moisture content reduction X/X_0 during the drying process, approximated as

$$\frac{V(t)}{V_0} = 1 - 0.276\big(X_0 - X(t)\big) \ . \tag{7}$$

After complete drying, the final moisture content $X_d = 0.076$ was evaluated and the resulting rescaled dry-sample volume attains the value $V_d/V_0 \simeq 0.68$. The larger shrinkage, also in this case, may be due to a significantly higher initial moisture content X_0.

The equilibrium water volume fraction ϕ_{eq} can be evaluated, from the equilibrium X_{eq} and initial X_0 moisture contents and the rescaled dry-sample volume V_d/V_0, as follows

$$\phi_{eq} = \phi_0 \left(\frac{X_{eq}}{X_0}\right)\left(\frac{V_d}{V_0}\right)^{-1} \tag{8}$$

where the sample volume at equilibrium V_{eq} was approximated with the dry-sample volume V_d. For both data sets (1) and (2), the rescaled equilibrium moisture content X_{eq}/X_0 is assumed $X_{eq}/X_0 = 0.055$ (kg/kg db) in agreement with the asymptotic value of the rescaled moisture content derived from dehydration curves of cocoa beans reported in [9,10] analyzed in Sections 4.1 and 4.2. The resulting values are $\phi_{eq} \simeq 0.038$ for data set (1) and $\phi_{eq} \simeq 0.041$ for data set (2).

All these physical and morphological parameters a_0, b_0, c_0, λ_0, V_0^{core}/V_0, V_0^{shell}/V_0, V_d/V_0, ϕ_0, ϕ_0^{core}, ϕ_0^{shell} and ϕ_{eq} are needed to implement the moving-boundary model for isothermal dehydration, presented and analyzed in Section 3.

3. Mathematical Models

In this section, we briefly review the basic equations of the moving-boundary model for food isothermal dehydration, developed in [13,14].

The transport equation describing the space-time evolution of the pointwise water concentration $c_w(\mathbf{x}, t)$ inside the bean, whose volume $V(t)$ and surface $S(t)$ are evolving in time, is the following advection-diffusion equation accounting for the local shrinkage through the pointwise shrinkage velocity $\mathbf{v}(\mathbf{x})$

$$\frac{\partial c_w(\mathbf{x}, t)}{\partial t} + \nabla \cdot \Big(\mathbf{v}(\mathbf{x})\, c_w(\mathbf{x}, t)\Big) = -\nabla \cdot \mathbf{J} = \nabla \cdot \big(D\, \nabla c_w(\mathbf{x}, t)\big)\,, \quad \mathbf{x} \in V(t) \tag{9}$$

where $c_w(\mathbf{x}, t)$ is the mass concentration of water, $\mathbf{J} = -D\,\nabla c$ is the diffusive mass flux and $\nabla \cdot (c\mathbf{v})$ is a convective term arising from local shrinkage.

By enforcing the analogy between the dehydration process, in which the sample is releasing water, and the swelling process of rubbery polymers, in which the sample is absorbing water, the pointwise shrinkage velocity $\mathbf{v}$ is assumed proportional (and opposite in sign) to the diffusive (volumetric) flux $\mathbf{J}(\mathbf{x})/\rho_w$

$$\mathbf{v} = -\alpha(c_w)\mathbf{J}(\mathbf{x})/\rho_w = \alpha(c_w) D\, \nabla c_w/\rho_w\,, \tag{10}$$

where $\alpha(c_w)$ is a shrinkage proportionality factor, depending on the pointwise water concentration.

The shrinkage factor $\alpha(c_w)$ is the fingerprint of the specific food material under investigation. The simplest case is that of a constant value, i.e., $\alpha(c_w) = \alpha_0$. $\alpha_0 = 0$ represents the case of a fully rigid solid (no shrinkage). $\alpha_0 = 1$ represents the case of *ideal* shrinkage, in which volume reduction corresponds exactly to the volume of water flowing outside the system. Values of α_0 less or greater than unity imply volume reduction less or greater than the corresponding water volume flow, respectively.

It must be observed that the assumption $\alpha(c_w) = \alpha_0$ does not imply that the shrinkage velocity $\mathbf{v}(\mathbf{x})$ is constant but rather that, according to Equation (10), the shrinkage velocity is directly proportional to the local concentration gradient. Therefore, the shrinkage velocity asymptotically tends to zero, at each point in the sample, when equilibrium conditions are reached and the water concentration gradient is null everywhere in the system.

The shrinkage velocity $\mathbf{v}(\mathbf{x})$ also controls the temporal evolution of the sample boundary $S(t)$ that evolves in time according to the following equation

$$\frac{d\mathbf{x}_b}{dt} = \mathbf{v}\big|_{\mathbf{x}_b} = \frac{\alpha(c_w)}{\rho_w} D\, \nabla c_w|_{\mathbf{x}_b}\,, \quad \mathbf{x}_b \in S(t)\,. \tag{11}$$

The two transport equations Equations (9) and (11) are linked together and must be solved simultaneously by further enforcing the following boundary conditions accounting for the flowing water from the boundary $S(t)$ towards the environment

$$-D\,\nabla c_w\cdot\mathbf{n}\big|_{\mathbf{x}_b}=h_m\,\rho_{air}\left(Y|_{\mathbf{x}_b}-Y_{eq}\right)=h_m\,\rho_{air}\frac{K_{eq}}{\rho_s}\left(c_w\big|_{\mathbf{x}_b}-c_{w,eq}\right)\ ,\quad \mathbf{x}_b\in S(t) \tag{12}$$

where $\mathbf{n}$ is the outward-pointing normal unit vector, h_m is a mass transfer coefficient (m/s), Y is the air moisture content (kg water/kg dry air), ρ_{air} is the air density on dry basis (kg dry air/m^3), ρ_s is the solid (pulp) density (kg pulp/m^{3}product) and K_{eq} is the water partition ratio between the gas and the solid phases $Y=K_{eq}\,c/\rho_s$. The subscript eq stands for equilibrium values.

By introducing the water volume fraction $\phi(\mathbf{x})=c_w(\mathbf{x})/\rho_w$, the dimensionless space and time variables $\tau=tD/L_r^2$, $\widetilde{\mathbf{x}}=\mathbf{x}/L_r$, $\widetilde{V}=V/L_r^3$, $\widetilde{S}=S/L_r^2$ and the dimensionless differential operators $\widetilde{\nabla}=\nabla/L_r$, $\widetilde{\nabla}\cdot=\frac{\nabla}{L_r}\cdot$, L_r being a characteristic reference length, the moving-boundary model equations attain the form:

$$\frac{\partial\phi}{\partial\tau}=\widetilde{\nabla}\cdot\Big(\widetilde{\nabla}\phi-\left(\alpha\nabla\phi\right)\phi\Big)=\widetilde{\nabla}\cdot\Big(\widetilde{\nabla}\phi\,(1-\alpha\phi)\Big)\ ,\quad \widetilde{\mathbf{x}}\in\widetilde{V}(\tau) \tag{13}$$

$$-\widetilde{\nabla}\phi\cdot\mathbf{n}|_{\widetilde{\mathbf{x}}_b}=Bi_m\left(\phi|_{\widetilde{\mathbf{x}}_b}-\phi_{eq}\right)\ ,\quad \widetilde{\mathbf{x}}_b\in\widetilde{S}(t) \tag{14}$$

$$\frac{d\widetilde{\mathbf{x}}_b}{d\tau}=\alpha\widetilde{\nabla}\phi|_{\widetilde{\mathbf{x}}_b}\ ,\quad \widetilde{\mathbf{x}}_b\in\widetilde{S}(\tau) \tag{15}$$

where $\alpha=\alpha(\phi)$ is the shrinkage factor and Bi_m is the mass transfer Biot number

$$Bi_m=\frac{h_mL_r}{D}K_{eq}\frac{\rho_{air}}{\rho_s}\ . \tag{16}$$

Initial conditions are $\widetilde{V}(0)=\widetilde{V}_0$, $\widetilde{S}(0)=\widetilde{S}_0$ and $\phi(\widetilde{\mathbf{x}},0)=\phi_0(\widetilde{\mathbf{x}})$.

In the next three paragraphs the moving-boundary model is applied to ellipsoidal beans in order to investigate:

1. the influence of the ellipsoidal shape on dehydration kinetics in the simplest case of a uniform initial water distribution, i.e., $\phi_0(\widetilde{\mathbf{x}})=$ constant and in the absence of shrinkage, i.e., $\alpha(\phi)=0$;
2. the influence of a nonuniform initial water distribution, i.e., $\phi_0(\widetilde{\mathbf{x}})=\phi_0^{core}$ for $\widetilde{\mathbf{x}}\in\widetilde{V}^{core}$ and $\phi_0(\widetilde{\mathbf{x}})=\phi_0^{shell}$ for $\widetilde{\mathbf{x}}\in\widetilde{V}^{shell}$, on dehydration rates, in the absence of shrinkage, $\alpha(\phi)=0$;
3. the influence, on dehydration rates, of a constant shrinkage factor $\alpha(\phi)=\alpha_0$.

The ellipsoidal beans analyzed in the next three paragraphs have the three principal axes $a_0=25$ mm, $b_0=13$ mm, $c_0=9$ mm and the shell thickness is $\lambda_0=0.5$ mm, an therefore the ratio $V_0^{core}/V_0\simeq 0.787$. The reference length is $L_r=c_0=9$ mm and the initial water volume fraction (averaged over the entire bean, shell and core) is $\phi_0=0.5$.

The 3-d moving-boundary model was numerically solved using finite elements method (FEM) in COMSOL Multiphysics® v. 3.5. (COMSOL AB, Stockholm, Sweden). The convection-diffusion package (conservative form) was coupled with ALE (Arbitrary Lagrangian Eulerian) moving mesh, allowing re-meshing during the time evolution of the physical domain. Free displacement induced by boundary velocity conditions was set. Lagrangian quadratic elements were chosen. The linear solver adopted is UMFPACK, with relative tolerance 10^{-3} and absolute tolerance 10^{-6}. The number of finite elements was 4×10^5–6×10^5 with a non-uniform mesh. Smaller elements (minimum element size 0.01 dimensionless unit) have been located close to the moving boundary and to the core/shell boundary in order to accurately compute concentration gradients controlling the velocity of the moving front and the water transport at the core/shell interface. Figure 3 shows the computational domain (1/4 of the ellipsoidal bean) and the FEM mesh adopted.

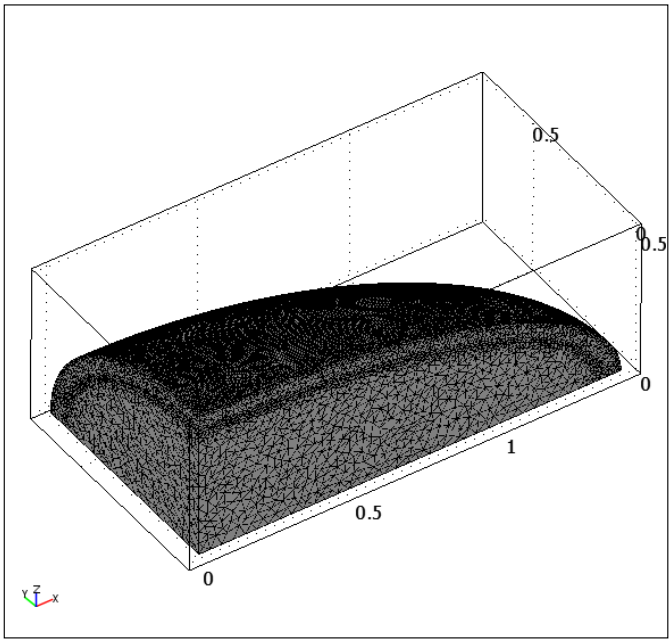

Figure 3. Representation of the computational domain (1/4 of the ellipsoidal bean) and the FEM (finite elements method) mesh adopted.

3.1. Uniform Initial Water Distribution (No Shrinkage)

If we assume no volume shrinkage, i.e., $\alpha(\phi) = 0$ and $\mathbf{v}(\widetilde{\mathbf{x}}) = 0$, the transport equation Equation (13) is a pure diffusion equation on a fixed 3-d domain $\widetilde{V}(\tau) = \widetilde{V}_0$, to be solved with the boundary condition Equation (14) on a fixed surface $\widetilde{S}(\tau) = \widetilde{S}_0$. The uniform initial water distribution inside the bean implies $\phi(\widetilde{\mathbf{x}}, 0) = \phi_0^{core} = \phi_0^{shell} = \phi_0$ corresponding to unitary partition coefficients $\beta_0^{core} = \beta_0^{shell} = 1$, see Equation (4).

Figure 4A shows the behaviour of the moisture ratio $X_r = \frac{(X - X_{eq})}{(X_0 - X_{eq})}$ vs. the dimensionless time $\tau = \frac{tD}{L_r^2}$ for different values of the Biot number $Bi_m = 1, 2, 3, 5, 9$. Figure 4B shows the same data on a log-normal plot and the perfect agreement with the asymptotic exponential behaviour (dashed lines)

$$X_r = \frac{X - X_{eq}}{X_0 - X_{eq}} \sim \exp\left[-\gamma_0^2 \left(\frac{L_r}{R_{eq}} \right)^2 \tau \right] \quad \text{for large } \tau \tag{17}$$

where γ_0 is the smallest positive root of the equation [17,18]

$$\gamma \cot(\gamma) + Bi_m^{eq} - 1 = 0\,, \quad Bi_m^{eq} = Bi_m \left(\frac{R_{eq}}{L_r} \right) \tag{18}$$

and Bi_m^{eq} is the equivalent mass Biot number, i.e., the Biot number for a sphere with the same surface-to-volume ratio as the ellipsoidal bean, therefore a sphere with radius R_{eq}

$$\frac{4\pi R_{eq}^2}{(4/3)\pi R_{eq}^3} = \frac{S^{ellipsoid}}{V^{ellipsoid}} \rightarrow R_{eq} = 3\,\frac{V^{ellipsoid}}{S^{ellipsoid}} = 3\,\frac{(\pi/6)a_0 b_0 c_0}{4\pi \left(\frac{a_0^p b_0^p + a_0^p c_0^p + b_0^p c_0^p}{3} \right)^{1/p}} \tag{19}$$

where $p \simeq 1.6075$.

For the cocoa bean under investigation, $R_{eq} \simeq 6.3$ mm, $R_{eq}/L_r = R_{eq}/c_0 \simeq 0.7$ and therefore $Bi_m^{eq} \simeq 0.7 Bi_m$. The corresponding values of γ_0 for different values of Bi_m are reported in Table 2. It can

be observed that γ_0 is an increasing function of Bi_m and only in the limit of $Bi_m \to \infty$, meaning that the mass transfer resistance at the solid-air interface is negligible, then $\gamma_0 \to \pi$.

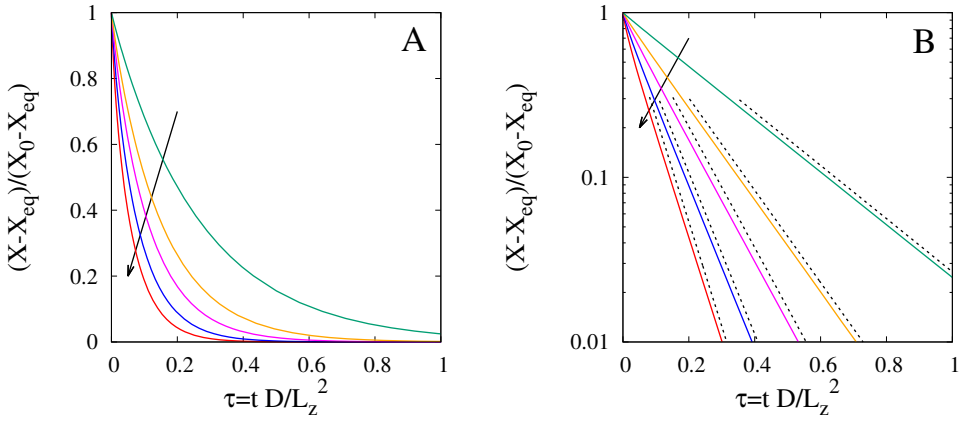

Figure 4. (**A**) Moisture ratio $(X - X_{eq})/(X_0 - X_{eq})$ vs. dimensionless time $\tau = tD/L_z^2$ for $Bi_m = 1, 2, 3, 5, 9$ and a uniform initial water distribution $\phi_0^{core} = \phi_0^{shell} = \phi_0 = 0.5$. (**B**) Log-normal plot of dehydration curves reported in Figure (**A**). Arrows indicate increasing values of Bi_m. Dashed black lines show the asymptotic theoretical exponential behaviour, Equations (17) and (18).

Table 2. Values of γ_0 for $R_{eq}/L_r = 0.7$ and different values of Bi_m.

	$Bi_m = 1$	$Bi_m = 2$	$Bi_m = 3$	$Bi_m = 5$	$Bi_m = 7$	$Bi_m = 9$
γ_0	1.35252	1.79058	2.06105	2.38064	2.56061	2.67429

Following reasonings similar to Paramo et al. [11], it is straightforward to verify that the exponential behaviour in Equations (17) and (18), which settles down for long/intermediate dehydration time-scales, implies a linear behaviour for the dimensionless dehydration rate J_d vs. X_r for small/intermediate values of X_r

$$J_d = -\frac{dX_r}{d\tau} = \gamma_0^2 \left(\frac{L_r}{R_{eq}}\right)^2 X_r \quad \text{for small } X_r \tag{20}$$

as shown in Figure 5.

Equation (20) can be used, in a direct way, to estimate the effective water diffusivity D from the initial linear scaling of the experimental dehydration-rate curves $j_d = -\frac{dX_r}{dt}$ vs. t. Indeed, by recalling that $\tau = tD/L_r^2$, Equation (20) can be rewritten as

$$j_d = -\frac{dX_r}{dt} = D\,\frac{\gamma_0^2}{R_{eq}^2} X_r \quad \text{for small } X_r \tag{21}$$

where γ_0 and R_{eq} are given by Equations (18) and (19), respectively and the only unknown quantity is D. However, the estimate of D from Equation (21) and from the initial slope δ (h^{-1}) of the experimental dehydration-rate curve $j_d = \delta X_r$ is not so straightforward as it requires the solution of a nonlinear equation for D because γ_0 is a nonlinear function of Bi_m and Bi_m depends on D itself, see Equation (16).

Equation (17), or equivalently Equation (20), implies that the dehydration curve of an ellipsoidal bean, on intermediate/long time-scales, can be very accurately approximated by the dehydration curve of a spherical bean with the same surface-to-volume ratio, i.e., with an equivalent radius R_{eq} given by Equation (19).

This finding gives an ultimate answer to the recurring question about how to approximate an ellipsoidal bean for solving the transport equations in a simplified geometry. For example, Herman et al. [9] approximated the ellipsoidal cocoa bean with a cylinder (see Section 2 for details).

Koua et al. [7], following Delgato et al. [19], and Chayjan and Kaveh [20], approximated the ellipsoidal bean with a sphere with the geometric mean radius $R_g = \frac{1}{2}(a\,b\,c)^{1/3}$. For the ellipsoidal bean under investigation, $R_g \simeq 7.15$ mm that is significantly larger than the equivalent radius $R_{eq} \simeq 6.3$ mm evaluated from Equation (19). The adoption of R_g instead of R_{eq} in Equation (21) would lead to an overestimate of the effective diffusivity D by a factor $(R_g/R_{eq})^2 \simeq 1.288$ and therefore to a percentage error of about 28%, and this without considering the further error in the overestimation of the equivalent Biot number Bi_m^{eq}, and therefore of γ_0, Equation (18).

Ndukwu et al. [21], following Asoegwu [22] proposed to approximate the ellipsoidal bean with a sphere with an equivalent radius $R_{av} = \frac{1}{3}(R_g + R_a + R_s)$ given by the average between the geometric mean radius $R_g = \frac{1}{2}(a\,b\,c)^{1/3}$, the arithmetic mean radius $R_a = \frac{1}{6}(a + b + c)$ and the square mean radius $R_s = \frac{1}{2}[(a\,b + b\,c + a\,c)/3]^{1/2}$. For the ellipsoidal bean under investigation, $R_{av} \simeq 7.48$ mm, even bigger that R_g and this would lead to an overestimation error for D of about 41%.

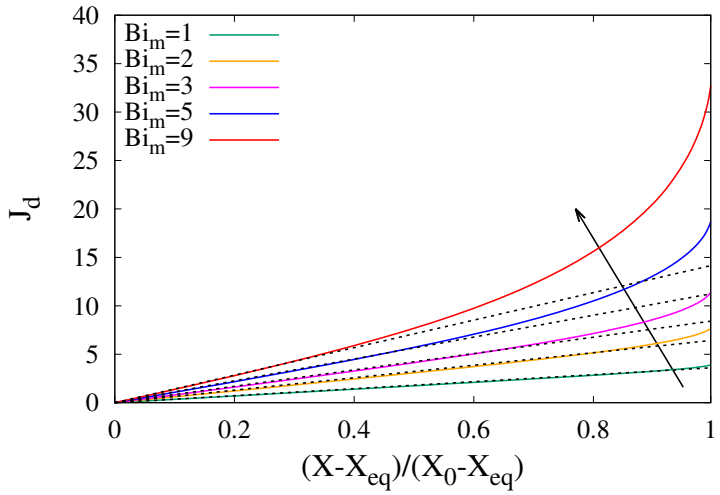

Figure 5. Dimensionless dehydration rate J_d vs. moisture ratio $X_r = (X - X_{eq})/(X_0 - X_{eq})$ for $Bi_m = 1, 2, 3, 5, 9$ for a uniform initial water distribution, $X_0^{core}/X_0 = V_0^{core}/V_0$. Arrow indicates increasing values of Bi_m. Dashed lines indicate the theoretical long-drying time-scales linear behaviour, Equation (20).

3.2. Non-Uniform Initial Water Distribution (No Shrinkage)

In this paragraph, the influence of a non-uniform initial water distribution on dehydration-rate curves is investigated, in the absence of bean shrinkage, i.e., $\alpha(\phi) = 0$.

Also in this case, as in Section 3.1, the transport equation Equation (13) is pure diffusion equation on a fixed 3-d domain $\widetilde{V}(\tau) = \widetilde{V}_0$, to be solved with the boundary condition Equation (14) on a fixed surface $\widetilde{S}(\tau) = \widetilde{S}_0$. What changes is the initial condition for the water distribution, because in this case $\phi(\widetilde{\mathbf{x}}, 0) = \phi_0^{core}$ for $\widetilde{\mathbf{x}} \in \widetilde{V}^{core}$ and $\phi(\widetilde{\mathbf{x}}, t) = \phi_0^{shell}$ for $\widetilde{\mathbf{x}} \in \widetilde{V}^{shell}$, with $\phi_0^{core} \neq \phi_0^{shell}$.

Specifically, we analyze two different initial conditions, namely $\beta_0^{core} = 0.9$ (that implies $\beta_0^{shell} \simeq 1.35$) and $\beta_0^{core} = 0.8$ (that implies $\beta_0^{shell} \simeq 1.74$), both corresponding to the case in which $\phi_0^{shell} > \phi_0^{core}$.

Figure 6 shows the dimensionless dehydration rate J_d vs. the moisture ratio X_r for different values of Bi_m, for a uniform initial water distribution, $\beta_0^{core} = \beta_0^{shell} = 1$ (continuous lines) and for the two non-uniform initial water distributions (dashed lines), $\beta_0^{core} = 0.9, 0.8$. The higher the value of water concentration in the shell ϕ_0^{shell}, the faster the decrease of the total moisture content at the beginning of the drying process, and therefore the larger the initial dehydration rate J_d. The larger the Bi_m, the larger the influence of initial water non-uniformity on dehydration-rate curves.

It should be further observed that in the absence of shrinkage, the linear scaling of J_d vs. X_r for small X_r (long dehydration time-scales) is almost unaffected by the initial non-uniform water

distribution so that Equation (21) can be still applied to estimate the effective water diffusion coefficient D.

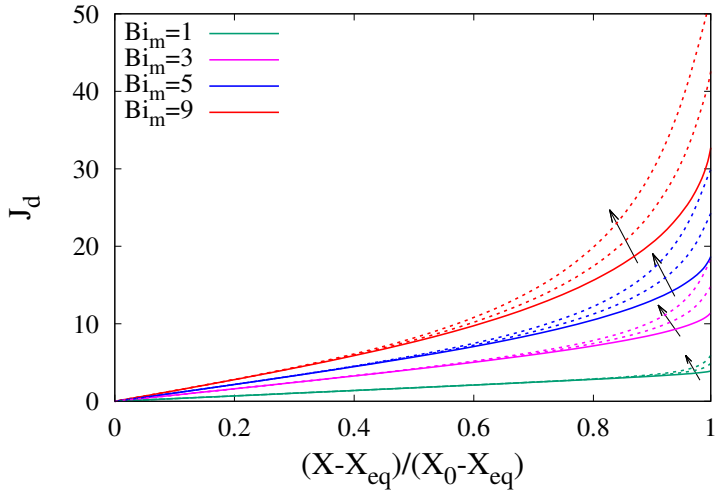

Figure 6. Dimensionless dehydration rate J_d vs. moisture ratio $X_r = (X - X_{eq})/(X_0 - X_{eq})$ for $Bi_m = 1, 3, 5, 9$ for a uniform initial water distribution, $\beta_0^{core} = \beta_0^{shell} = 1$ (continuous lines) and for two non-uniform initial water distributions (dashed lines), $\beta_0^{core} = 0.9, 0.8$. Arrows indicate decreasing values of β_0, i.e., increasing non-uniformity.

3.3. The Influence of Shrinkage on Dehydration Curves

Sample shrinkage strongly influences the dehydration curves because the progressive decrease in volume leads to a reduction of the diffusional paths. If the water diffusivity D is assumed to be independent of the local water concentration, shrinkage accelerates the dehydration process and dehydration rates are higher.

Figure 7 shows the behaviour of the dehydration-rate curves for different values of Bi_m and increasing values of a constant shrinkage factor $\alpha(\phi) = \alpha_0 = 0, 0.1, 0.3, 0.5$. The dehydration-rate curves shown in Figure 7 was obtained by numerically integrating the moving-boundary transport model Equations (13)–(15) for a uniform initial water distribution $\phi(\tilde{\mathbf{x}}, 0) = \phi_0^{core} = \phi_0^{shell} = \phi_0$.

The assumption of a constant shrinkage factor $\alpha(\phi) = \alpha_0$ does not imply a constant shrinkage velocity but rather that the pointwise shrinkage velocity is proportional to the local water concentration gradient with a proportionality constant that is uniform inside the sample and constant during the course of the dehydration process.

A constant shrinkage factor $\alpha(\phi) = \alpha_0$ implies a linear "calibration curve", i.e., a linear relationship between volume reduction $[1 - \frac{V(t)}{V_0}]$ and moisture content reduction $[1 - \frac{X(t)}{X_0}]$

$$\left[1 - \frac{V}{V_0}\right] = \alpha_0 \phi_0 \left[1 - \frac{X}{X_0}\right] \longrightarrow \frac{V_{eq}}{V_0} = 1 - \alpha_0 \phi_0 \left(1 - \frac{X_{eq}}{X_0}\right). \tag{22}$$

When the moisture content reaches its asymptotic/equilibrium value X_{eq} and $X_{eq} \ll X_0$, the final sample volume V_{eq}/V_0 can be approximated as $V_{eq}/V_0 \simeq 1 - \alpha_0 \phi_0$.

The different dehydration-rate curves, shown in Figure 7, obtained for increasing values of α_0, from $\alpha_0 = 0$ (no shrinkage) to $\alpha_0 = 0.5$, correspond to decreasing values of the final sample volume, namely $V_{eq}/V_0 = 1, 0.95, 0.85, 0.75$, the latter two values very close to that observed from experimental cocoa bean shrinkage data (see Section 2). As expected, the higher α_0, the higher the dehydration rates, and this effect is amplified for higher Bi_m values.

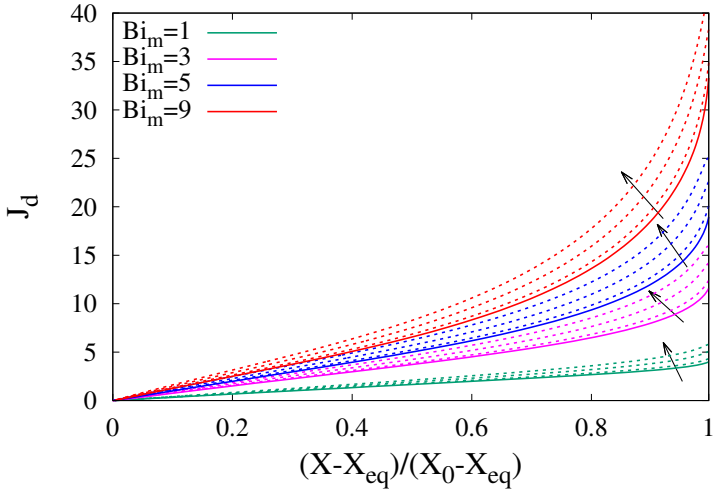

Figure 7. Dimensionless dehydration rate J_d vs. moisture ratio $X_r = (X - X_{eq})/(X_0 - X_{eq})$ for $Bi_m = 1, 3, 5, 9$ and for a uniform initial water distribution, $\beta_0^{core} = \beta_0^{shell} = 1$. Continuous lines: no-shrinkage. dashed lines: shrinkage factor $\alpha(\phi) = \alpha_0 = 0.1, 0.3, 0.5$. Arrows indicate increasing values of α_0.

It can be further observed that shrinkage also affects the linear scaling of J_d vs. X_r for small X_r (long dehydration time-scales). In the presence of shrinkage, this linear scaling can still be estimated from Equations (18) and (20), valid in the absence of shrinkage, by simply replacing the equivalent radius R_{eq} with the equivalent radius $\widetilde{R}_{eq} = R_{eq}(\frac{V_{eq}}{V_0})^{1/3}$, in which enters the factor $(\frac{V_{eq}}{V_0})^{1/3}$, accounting for volume reduction on longer time-scales, thus obtaining

$$J_d = \widetilde{\gamma}_0^2 \left(\frac{L_r}{\widetilde{R}_{eq}}\right)^2 X_r = \widetilde{\gamma}_0^2 \left(\frac{L_r}{R_{eq}}\right)^2 \left(\frac{V_{eq}}{V_0}\right)^{-2/3} X_r \quad \text{for small } X_r \tag{23}$$

where $\widetilde{\gamma}_0^2$ is the smallest positive root of the equation

$$\widetilde{\gamma}\cot(\widetilde{\gamma}) + \widetilde{Bi}_m^{eq} - 1 = 0\,, \quad \widetilde{Bi}_m^{eq} = Bi_m\left(\frac{\widetilde{R}_{eq}}{L_r}\right) = Bi_m\left(\frac{R_{eq}}{L_r}\right)\left(\frac{V_{eq}}{V_0}\right)^{1/3} \tag{24}$$

Figure 8 shows the excellent agreement between the dehydration-rate curves for $\alpha_0 = 0.5$ and the theoretical linear behaviour, Equations (23) and (24) with $R_{eq}/L_r = 0.7$, $V_{eq}/V_0 \simeq 0.85$ and with the values of $\widetilde{\gamma}_0$, derived from Equation (24), reported in Table 3.

Table 3. Values of $\widetilde{\gamma}_0$ for $R_{eq}/L_r = 0.7$, $\alpha_0 = 0.5$, $V_{eq}/V_0 = 0.85$ and different values of Bi_m.

	$Bi_m = 1$	$Bi_m = 2$	$Bi_m = 3$	$Bi_m = 5$	$Bi_m = 7$	$Bi_m = 9$
$\widetilde{\gamma}_0$	1.29016	1.71879	1.98915	2.31671	2.50135	2.62754

Therefore, also in the presence of shrinkage, the effective water diffusivity D can be estimated from the slope δ (h^{-1}) of the initial linear scaling of the experimental dehydration-rate curve $j_d = \delta X_r$ by solving the nonlinear equation for D

$$\delta = D\left(\frac{\widetilde{\gamma}_0}{R_{eq}}\right)^2 \left(\frac{V_{eq}}{V_0}\right)^{-2/3} \tag{25}$$

where $\widetilde{\gamma}_0$ depends on Bi_m and Bi_m depends on D, Equation (16).

In the next section we make a direct use of Equation (25) to estimate the effective water diffusivity D in cocoa beans by analyzing the experimental dehydration curves reported by Herman et al. [9,10].

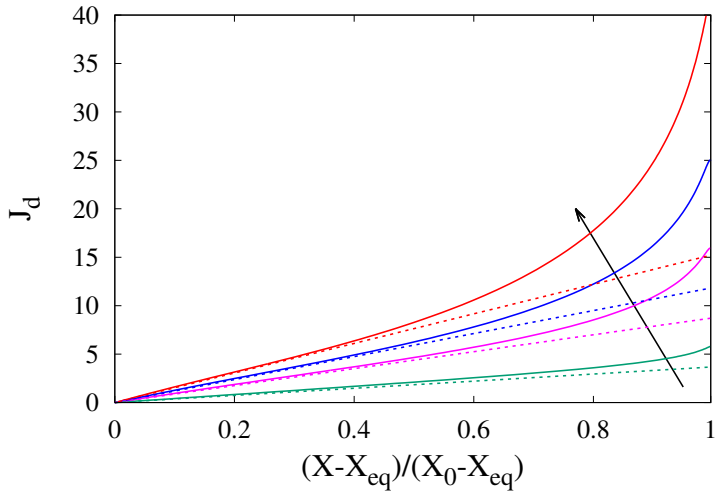

Figure 8. Dimensionless dehydration rate J_d vs. moisture ratio $X_r = (X - X_{eq})/(X_0 - X_{eq})$ for $Bi_m = 1, 3, 5, 9$ and for a uniform initial water distribution, $\beta_0^{core} = \beta_0^{shell} = 1$. Shrinkage factor $\alpha_0 = 0.5$, $V_{eq}/V_0 \simeq 0.85$. Arrow indicates increasing values of Bi_m. Dashed lines indicate the theoretical long-drying time-scales linear behaviour, Equation (23).

4. Analysis of Dehydration Kinetics and Shrinkage of Ellipsoidal Cocoa Beans

We analyze the experimental dehydration curves of ellipsoidal fermented Amazonian cocoa beans reported by Herman et al. [9,10] and verify the capability of the moving-boundary model, accounting for nonuniform initial water distribution inside the core and the shell and sample shrinkage, to describe and capture all the complex features of the dehydration kinetics of cocoa beans.

The shrinkage factor $\alpha(\phi)$ was assumed constant $\alpha(\phi) = \alpha_0$ and estimated from Equation (22) for both data sets. A review of all the physical, geometrical and shrinkage parameters adopted in the moving-boundary model for the analysis of data set (1) and (2) are reported in Table 4.

Table 4. Review of physical, geometrical and shrinkage parameters adopted in the moving-boundary model for the analysis of data set (1) and (2).

Data Set	ϕ_0 Equation (2)	R_{eq} (mm) Equation (19)	β_0^{core} Equation (4)	β_0^{shell} Equation (4)	V_{eq}/V_0 Equations (5) & (6)	ϕ_{eq} Equation (8)	α_0 Equation (22)
(1)	0.57	6.23	0.912	1.35	0.82	0.038	0.33
(2)	0.59	6.13	0.78	1.53	0.78	0.042	0.39

In Section 4.1, the effective water diffusivity D, at different drying temperatures, is estimated, starting from the experimental dehydration curves for cocoa beans characterized by a lower non-uniformity of the initial water distribution between core and shell, data set (1).

In Section 4.2 the moving-boundary model is adopted, in a fully predictive way, to evaluate the dehydration curves for different air velocities for cocoa beans of data set (1). Moreover, the moving-boundary model is applied to predict the dehydration curves for cocoa beans characterized by a higher non-uniformity of the initial water distribution and a larger shrinkage (data set (2)).

In Section 4.3 a detailed comparison between model predictions and experimental data for the temporal evolution of the moisture content and thickness of core and shell is presented. The influence of shrinkage is addressed in detail.

4.1. Estimate of Water Effective Diffusivity D

Figure 9A,B show the influence of the drying temperature on the dehydration kinetics of cocoa beans of data set (1) for a fixed air velocity $v = 0.6$ m/s. Figure 9A shows the temporal decay of

the rescaled moisture content $X(t)/X_0$ of the entire bean (core and shell) while Figure 9B shows the behaviour of the dimensional dehydration rate j_d (h^{-1}) vs. X_r. For each temperature T, the dehydration-rate curve j_d vs. X_r has been obtained from a best fit of the dehydration curve X/X_0 vs. t, at the same temperature T, with the following function

$$X(t)/X_0 = a_0 + a_1 e^{-b_1 t} + a_2 e^{-b_2 t} + (1 - a_0 - a_1 - a_2) e^{-b_3 t} ,$$

superposition of three exponential functions of time plus a constant and satisfying the two constrains $X(0)/X_0 = 1$, $X_{eq}/X_0 = a_0$;

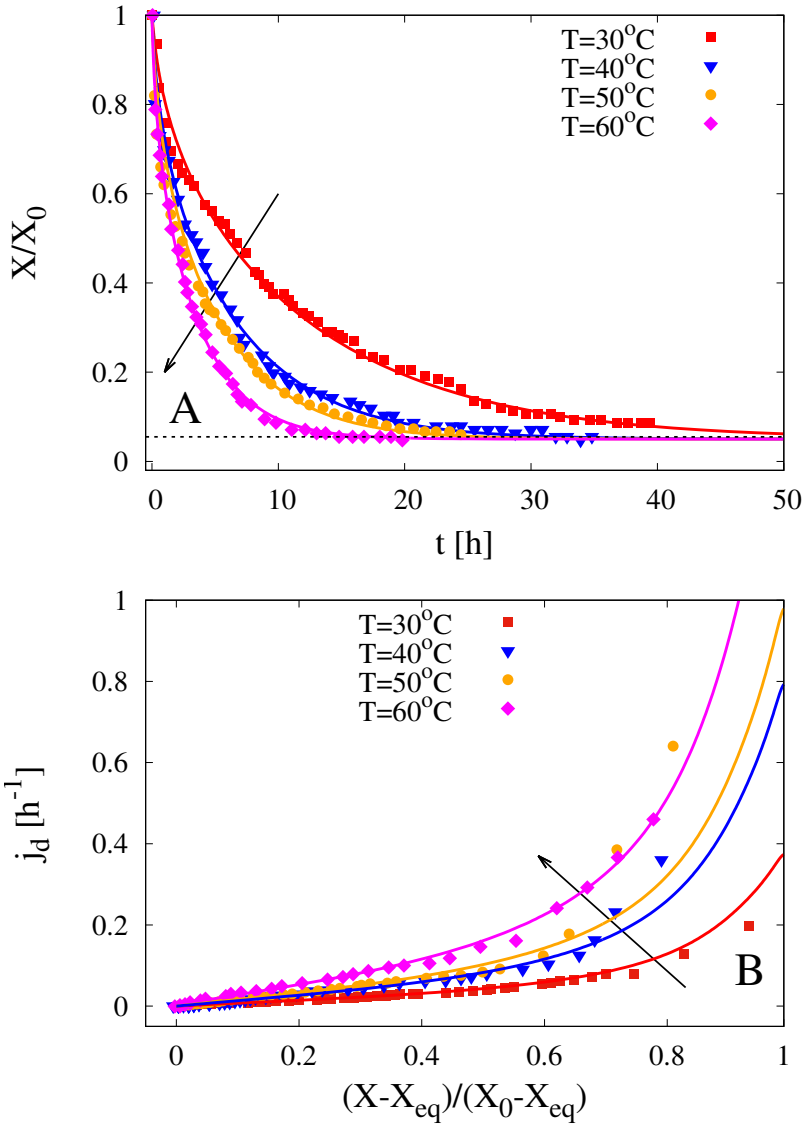

Figure 9. (**A**) Dehydration curves X/X_0 vs. t (h) and (**B**) dehydration-rate curves j_d (h^{-1}) vs. X_r for $T = 30$ °C, 40°C, 50 °C, 60 °C and $v = 0.6$ m/s. Cocoa bean from data set (1). Comparison between experimental data (points) and model predictions (continuous lines) with water diffusivities D and Biot numbers Bi_m reported in Table 5. Arrows indicate increasing values of T. Dashed line indicates the asymptotic rescaled moisture content $X_{eq}/X_0 = 0.055$.

The dehydration rate $j_d(t)$ has been subsequently evaluated as

$$j_d = -\frac{dX_r}{dt} = -\frac{d}{dt}\left[\frac{X - X_{eq}}{X_0 - X_{eq}}\right] = \frac{d(X/X_0)}{dt}\frac{-1}{1 - X_{eq}/X_0},$$

hence

$$j_d = \frac{1}{1 - a_0}\left(a_1 b_1 e^{-b_1 t} + a_2 b_2 e^{-b_2 t} + (1 - a_0 - a_1 - a_2)\, b_3 e^{-b_3 t}\right),$$

plotted as a function of $X_r = \frac{(X(t)/X_0) - a_0}{1 - a_0}$.

As expected, the synergistic effect of a larger moisture content in the shell and of shrinkage leads to high values of the dehydration rate at the beginning of the drying process (large X_r) and a rapid decrease of j_d towards the asymptotic linear scaling $j_d = \delta(T)X_r$, valid for smaller values of X_r.

From the experimental values of $\delta(T)$ and Equation (25), it is possible to evaluate the minimum value of the water diffusivity $D_{min}(T)$ at different temperatures, i.e., the value of the water diffusivity that would be estimated if the mass transfer resistance at the solid/air interface were neglected. Indeed, $D_{min}(T)$ can be readily estimated from $\delta(T)$ and Equation (25) by assuming $h_m \to \infty$, which implies $Bi_m \to \infty$ and therefore $\gamma_0 \to \pi$. The value of the actual water diffusivity $D(T)$ is necessarily greater than $D_{min}(T)$ because, for any finite value of Bi_m, $\gamma_0 < \pi$.

The values of D_{min}, together with the optimized values of D (and the corresponding Bi_m), obtained by a best fit of numerical data from the moving-boundary model onto the experimental data, for different drying temperatures, are reported in Table 5. The excellent agreement between the experimental data (points) and the numerical results of the moving-boundary model (continuous lines) is shown in Figure 9A and B both for the dehydration curves and the dehydration-rate curves.

Table 5. Estimated water diffusivities D_{min}, D and Biot number Bi_m for cocoa beans of data set (1) for different drying temperatures T and $v = 0.6$ m/s.

	$T = 30\,^{\circ}\mathrm{C}$	$T = 40\,^{\circ}\mathrm{C}$	$T = 50\,^{\circ}\mathrm{C}$	$T = 60\,^{\circ}\mathrm{C}$
D_{min} (m^2/s)	$(7.65 \pm 0.1) \times 10^{-11}$	$(1.34 \pm 0.03) \times 10^{-10}$	$(1.62 \pm 0.05) \times 10^{-10}$	$(2.48 \pm 0.03) \times 10^{-10}$
D (m^2/s)	$(9.11 \pm 0.1) \times 10^{-11}$	$(1.54 \pm 0.03) \times 10^{-10}$	$(2.09 \pm 0.05) \times 10^{-10}$	$(3.12 \pm 0.03) \times 10^{-10}$
Bi_m	(17.93 ± 0.1)	(16.24 ± 0.1)	(14.83 ± 0.1)	(13.61 ± 0.12)

The diffusivity values $D(T)$ are plotted in Figure 10, as a function of T, together with the Arrhenius function $D = D_0 \exp[-E/(RT)]$ with $D_0 = 5.77 \times 10^{-5}$ m^2/s and $E/R = 4037.78$ (K). These values are slightly larger than that reported by Herman et al. [9] ($D(T) \in [(6.8 \pm 0.17) \times 10^{-11} \div (1.41 \pm 0.19) \times 10^{-10}]$ m^2/s for $T \in [30\,^{\circ}\mathrm{C} \div 60\,^{\circ}\mathrm{C}]$) that are, however, all below the minimum values $D_{min}(T)$ reported in Table 5.

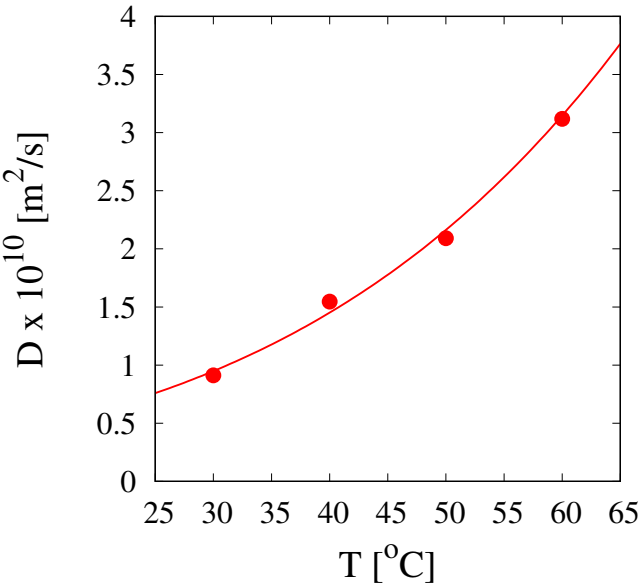

Figure 10. Diffusion coefficient D (m^2/s) vs. dehydration temperature T (°C). Continuous line represents the Arrhenius behaviour $D = D_0 \exp[-E/(RT)]$ with $D_0 = 5.77 \times 10^{-5}$ m^2/s and $E/R = 4037.78$ (K).

4.2. Influence of Air Velocity and Non-Uniformity of the Initial Water Distribution

The moving-boundary model is adopted, in a fully predictive way, to investigate the influence of air velocity of the dehydration kinetics.

Figure 11A and B show experimental data (points) for the dehydration curves X/X_0 vs. t (h) and for the dehydration-rate curves j_d vs. X_r at $T = 60$ °C for three different air velocities, $v = 0.3, 0.6, 1$ m/s, as reported by Herman et al. for cocoa beans of data set (1).

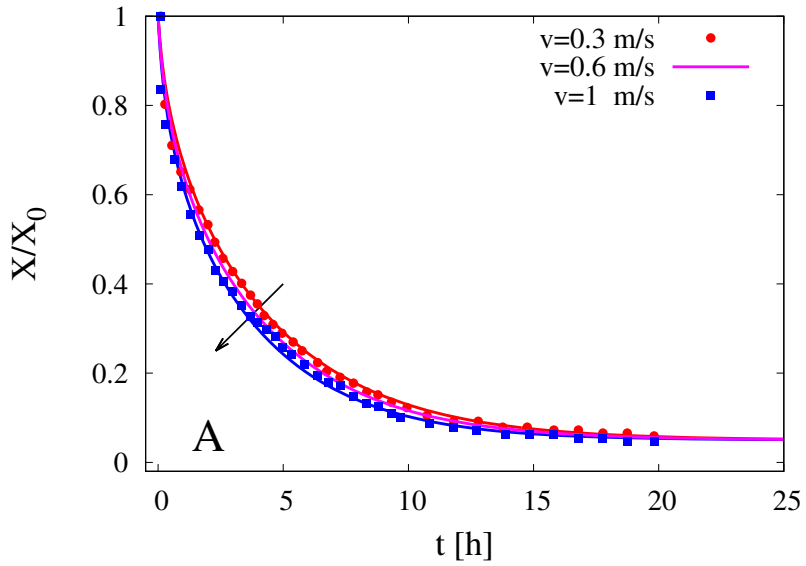

Figure 11. *Cont.*

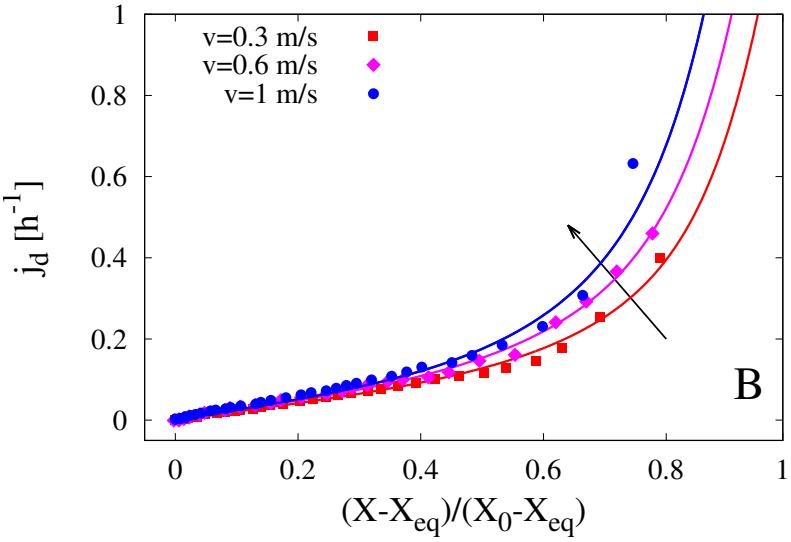

Figure 11. Influence of air velocity $v = 0.3, 0.6, 1$ m/s on dehydration kinetics at $T = 60$ °C. Comparison between experimental data and model predictions with $D = 3.12 \times 10^{-10}$ m^2/s and $Bi_m = 10.27, 13.61, 16.93$ for $v = 0.3, 0.6, 1.0$ m/s, respectively. Arrows indicate increasing values of v and Bi_m. (**A**) Rescaled moisture content X/X_0 vs. time (h). (**B**) Dehydration rate j_d (h^{-1}) vs. moisture ratio X_r.

Continuous lines are model predictions with $D(60\ ^\circ\text{C}) = 3.12 \times 10^{-10}$ m^2/s (see Table 5) and with different values of Bi_m, namely $Bi_m = 10.27, 13.61, 16.93$ for $v = 0.3, 0.6, 1$ m/s, respectively. The mass transfer coefficient h_m, entering the Bi_m number, was estimated, for different velocities v, from the classical Frössling correlation [23] for the Sherwood number, valid for spheres

$$Sh = 2 + 0.6 Re^{1/2} Sc^{1/3} \tag{26}$$

where the equivalent radius $R_{eq} = 6.23$ mm for cocoa beans of data set (1) was used both in the Sherwood number and in the Reynolds number.

The moving-boundary model accurately describes the sensitivity of the dehydration curves to the air velocity and quantitatively predicts the slight increase of the dehydration rates for increasing Reynolds numbers.

The moving-boundary model can also accurately predict the influence of the non-uniformity of the initial water distribution on the dehydration kinetics. Indeed, Figure 12 shows the excellent agreement between experimental dehydration kinetics and model predictions for both data set (1) (data already shown in Figure 9A,B) and data set (2) for $T = 60$ °C and $v = 0.6$ m/s. Cocoa beans of data set (2) are characterized by a larger shell moisture content $\beta_0^{shell} = 1.53$ and a slightly larger asymptotic shrinkage $V_{eq}/V_0 = 0.78$, if compared to that of data set (1), see Table 4. Both these features contribute to a faster initial decay of the rescaled moisture content $X(t)/X_0$ and therefore to larger initial dehydration rates, perfectly predicted by the moving-boundary model with the same value of the water diffusivity $D(60\ ^\circ\text{C}) = 3.12 \times 10^{-10}$ m^2/s and the mass Biot number $Bi_m = 12.87$ directly obtained from the value $Bi_m = 13.61$, previously evaluated for cocoa beans of data set (1), by replacing the reference length L_r and the equivalent radius R_{eq} of data set (1) with the corresponding values for data set (2), see Table 4. It should be further observed that the dehydration-rate curves, for both data sets (1) and (2), almost overlap one another on longer dehydration time-scales. This asymptotic behaviour, well captured by the moving-boundary model, is in agreement with what is expected by considering that the water diffusivity D may be assumed the same for both types of cocoa beans and also the equivalent radii R_{eq} for data set (1) and (2) are very close each other.

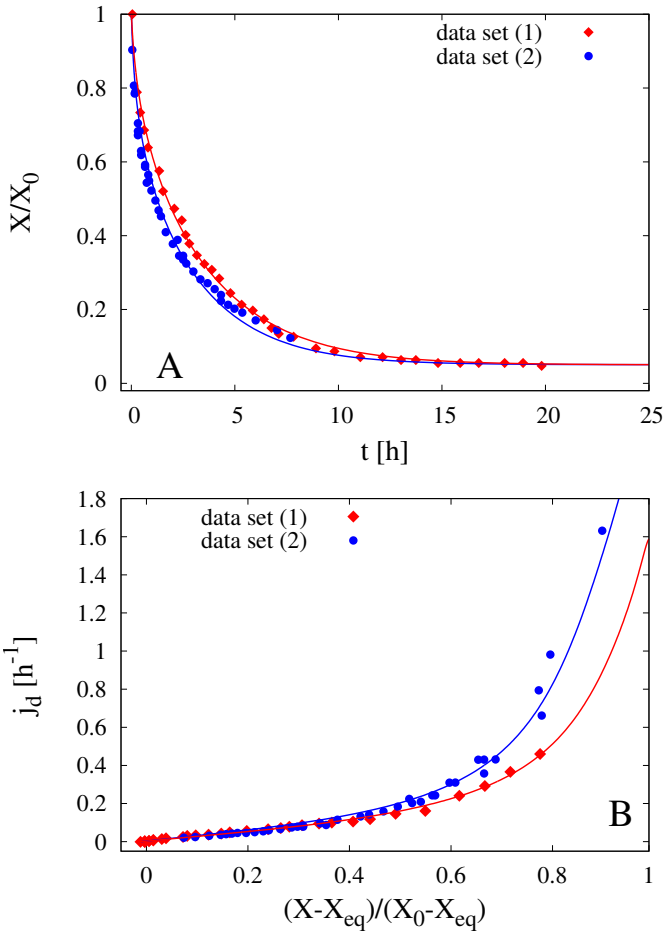

Figure 12. Dehydration kinetics at $T = 60$ °C and $v = 0.6$ m/s for two different types of cocoa beans (data set (1) and data set (2)), characterized by two different initial water distributions and final shrinkage, see Table 4. Comparison between experimental data and model predictions with $D = 3.12 \times 10^{-10}$ m^2/s and $Bi_m = 13.61$ for data set (1) and $Bi_m = 12.87$ for data set (2). (**A**) Rescaled moisture content X/X_0 vs. time (h). (**B**) Dehydration rate j_d (h^{-1}) vs. moisture ratio X_r.

4.3. Temporal Evolution of the Moisture Content and Thickness of Core and Shell

The moving-boundary model can accurately predict not only the temporal evolution of the total moisture content $X(t) = X^{core}(t) + X^{shell}(t)$ of the cocoa bean, but also the evolution, during the dehydration process, of the two specific moisture contents, namely that of the core X^{core} and of the shell X^{shell}, plotted as a function of the total moisture content X in Figure 13 for cocoa beans of data set (2), as reported by Herman et al. [10].

Continuous lines in Figure 13 show the model predictions for the moving-boundary model accounting for shrinkage, while dashed lines indicate model predictions without shrinkage. Both approaches give quite satisfactorily results but that accounting for shrinkage better describes the almost constant behaviour $X^{core} \simeq X_0^{core}$ at short/intermediate time scales, corresponding to $0.5 \leq X \leq X_0$. Both experimental data and theoretical results support the physical observation that the initial moisture content decay is mainly due to the dehydration of the bean shell.

In point of fact, although the volume contraction is not very large (about 30%), shrinkage effect must be necessarily taken into account for an accurate description of the dehydration curves and for a reliable estimate of the water diffusivity D.

The comparison between experimental data and model predictions for the evolution of the lengths of the three principal axes of the cocoa bean and of the shell thickness of data set (2), during

the dehydration process, is shown in Figure 14. It can be observed that, despite the extremely noisy experimental data of axes lengths and shell thickness, the model predictions can be considered quite satisfactory since they are able to capture general trends of all the quantities.

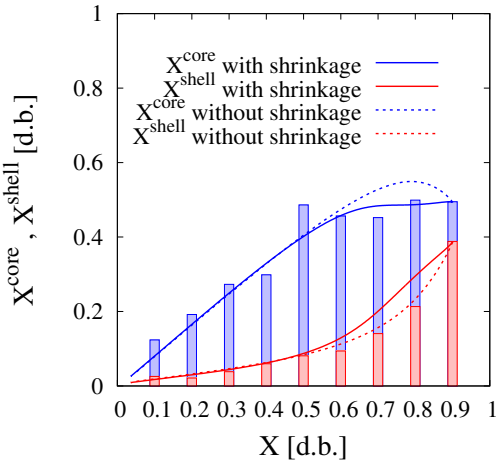

Figure 13. Moisture content in the core X^{core} and in the shell X^{shell} vs. the total moisture content $X = X^{core} + X^{shell}$ (kg/kg db) for cocoa beans of data set (2), $T = 60$ °C and $v = 0.6$ m/s. Comparison between experimental data (vertical bars) and model predictions (continuous and dashed lines) with $D = 3.12 \times 10^{-10}$ m^2/s, $Bi_m = 12.87$. Continuous lines indicate model predictions with a constant shrinkage factor $\alpha_0 = 0.39$. Dashed lines indicate model predictions without shrinkage $\alpha_0 = 0$.

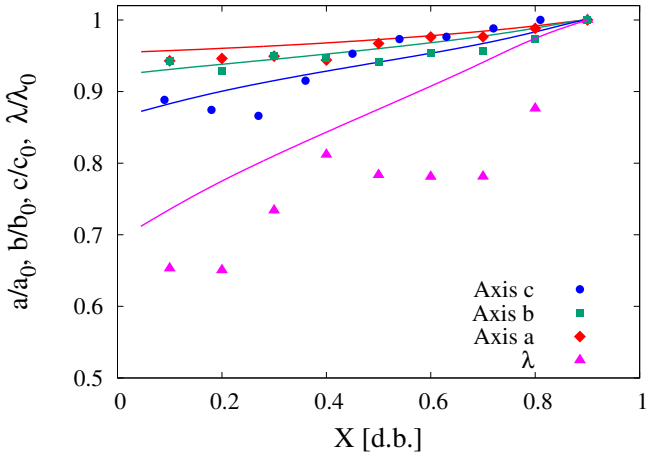

Figure 14. Rescaled lengths of the three principal axes and shell thickness vs. total moisture content $X = X^{core} + X^{shell}$ (kg/kg db) for cocoa beans of data set (2), $T = 60$ °C, $v = 0.6$ m/s. Comparison between experimental data and model predictions with $D = 3.12 \times 10^{-10}$ m^2/s, $Bi_m = 12.87$, $\alpha_0 = 0.39$.

Figure 15A–D show the evolution, during the drying process, of the water volume fraction $\phi(\tilde{\mathbf{x}}, t)$ inside the shrinking bean (shell and core), for decreasing values of the rescaled total moisture content $X(t)/X_0 = 1, 0.7, 0.3, 0.1$. The initial position of the external boundary (solid/air interface) and of the internal boundary (shell/core interface) are highlighted in order to have a better visualization of the progressive shrinkage of the bean.

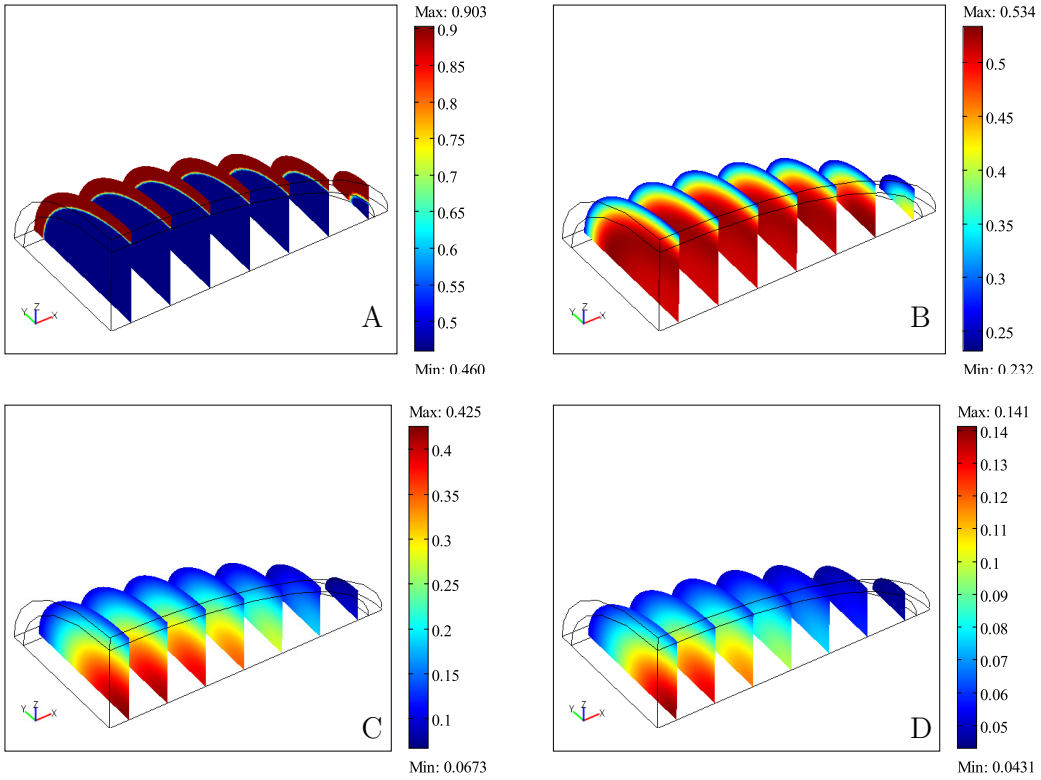

Figure 15. Evolution of the water volume fraction $\phi(\tilde{\mathbf{x}}, t)$ inside the shrinking bean (shell and core) for decreasing values of the rescaled total moisture content $X(t)/X_0$, $T = 60$ °C, $v = 0.6$ m/s, $D = 3.12 \times 10^{-10}$ m^2/s, $Bi_m = 12.87$, $\alpha_0 = 0.39$. **(A)** $X(t)/X_0 = 1$ (initial time instant); **(B)** $X(t)/X_0 = 0.7$; **(C)** $X(t)/X_0 = 0.3$; **(D)** $X(t)/X_0 = 0.1$.

5. Conclusions

The moving-boundary model for food isothermal dehydration, developed in [13,14], was applied to analyze the dehydration kinetics of ellipsoidal cocoa beans, characterized by a non-uniform initial distribution of the moisture content between the core and the shell.

The model proved capable of accurately describing the two-phases dehydration process: an initial fast dehydration of the shell, characterized by higher dehydration rates, followed by a slower dehydration of the core, characterized by a linear relationship $j_d = \delta(T)X_r$ between the dehydration rate j_d and the moisture ratio X_r.

Specifically, from this linear behaviour, a shortcut method to estimate the effective water diffusivity D is proposed, based on Equation (25), and derived from the basic observation that the asymptotic exponential behaviour of the dehydration curve $X_r(t)$ vs. t for an ellipsoidal bean coincides with that of an equivalent sphere, with radius R_{eq} given by Equation (19), with the same surface-to-volume ratio as the original ellipsoid.

The moving-boundary model was successfully applied to predict the influence of air velocity and non-uniformity of the initial water distribution on the dehydration rates, as well as to predict the temporal evolution of the water content in the core and in the shell and of the characteristic lengths of the ellipsoidal bean.

Author Contributions: Conceptualization, A.A. and A.B.; methodology, A.A. and A.B.; software, A.A. and A.B.; validation, A.A. and A.B.; formal analysis, A.A. and A.B.; investigation, A.A. and A.B.; resources, A.A.; data curation, A.A.; writing—original draft preparation, A.A.; writing—review and editing, A.B.; visualization, A.A. and A.B.; supervision, A.A.; project administration, A.A.; funding acquisition, A.A. All authors have read and agreed to the published version of the manuscript.

Funding: This research received no external funding. The APC was funded by INSTM Consorzio Interuniversitario Nazionale per la Scienza e Tecnologia dei Materiali.

Conflicts of Interest: The authors declare no conflict of interest.

References

1. Wollgast, J.; Anklam, E. Review on polyphenols in Theobroma cacao: Changes in composition during the manufacture of chocolate and methodology for identification and quantification. *Food Res. Int.* **2000**, *33*, 423–447. [CrossRef]
2. Hii, C.L.; Tukimon, M.B. Evaluation of fermentation techniques practiced by the cocoa smallholders. *Planter* **2002**, *78*, 13–22.
3. Hii, C.L.; Law, C.L.; Cloke, M. Modelling of thin layer drying kinetics of cocoa beans during artificial and natural drying. *J. Eng. Sci. Technol.* **2008**, *3*, 1–10.
4. Hii, C.L.; Law, C.L.; Cloke, M. Modeling using a new thin layer drying model and product quality of cocoa. *J. Food Eng.* **2009**, *90*, 191–198. [CrossRef]
5. Hii, C.L.; Law, C.L.; Cloke, M.; Suzannah, S. Thin layer drying kinetics of cocoa and dried product quality. *Biosyst. Eng.* **2009**, *102*, 153–161. [CrossRef]
6. Hii, C.L.; Law, C.L.; Law, M.C. Simulation of heat and mass transfer of cocoa bean under stepwise drying conditions in a heat pump dryer. *Appl. Ther. Eng.* **2013**, *54*, 264–271. [CrossRef]
7. Koua, B.K.; Koffi, P.M.E.; Gbaha, P. Evolution of shrinkage, real density, porosity, heat and mass transfer coefficients during indirect solar drying of cocoa beans. *J. Saudi Soc. Agric. Sci.* **2019**, *18*, 72–82. [CrossRef]
8. Okiyama D.C.G.; Navarro, S.L.B.; Rodrigues, C.E.C. Cocoa shell and its compounds: Applications in the food industry. *Trends Food Sci. Technol.* **2017**, *63*, 103–112. [CrossRef]
9. Herman, C.; Spreutels, L.; Turomza N.; Konagano, E.M.; Haut, B. Convective drying of fermented Amazonian cocoa beans (*Theobroma cacao* var. Forasteiro). Experiments and mathematical modelling. *Food Bioprod. Process.* **2018**, *108*, 81–94. [CrossRef]
10. Herman, C.; Fauvieau, J.; Haut B. Evolution of the moisture content in the core and the shell of fermented Amazonian cocoa beans during drying. In Proceedings of the EuroDrying 2019—7th European Drying Conference, Torino, Italy, 10–12 July 2019; pp. 158–165.
11. Páramo, D.; García-Alamilla, P.; Salgado-Cervantes, M.A.; Robles-Olvera, V.J.; Rodríguez-Jimenes, G.C.; García-Alvarado, M.A. Mass transfer of water and volatile fatty acids in cocoa beans during drying. *J. Food Eng.* **2010**, *99*, 276–283. [CrossRef]
12. Ruiz-López, I.I.; Córdova, A.V.; Rodríguez-Jimenes, G.C.; García-Alvarado, M.A. Moisture and temperature evolution during food drying: Effect of variable properties. *J. Food Eng.* **2004**, *63*, 117–124. [CrossRef]
13. Adrover, A.; Brasiello, A.; Ponso, G. A moving boundary model for food isothermal drying and shrinkage: General setting. *J. Food Eng.* **2019**, *244*, 178–191. [CrossRef]
14. Adrover, A.; Brasiello, A.; Ponso, G. A moving boundary model for food isothermal drying and shrinkage: A shortcut numerical method for estimating the shrinkage factor. *J. Food Eng.* **2019**, *244*, 212–219. [CrossRef]
15. Adrover, A.; Brasiello, A. A Moving Boundary Model for Isothermal Drying and Shrinkage of Chayote Discoid Samples: Comparison between the Fully Analytical and the Shortcut Numerical Approaches. *Int. J. Chem. Eng.* **2019**, *2019*, 3926897. [CrossRef]
16. Adrover, A.; Brasiello, A. A moving boundary model for food isothermal drying and shrinkage: One-dimensional versus two-dimensional approaches. *J. Food Process Eng.* **2019**, *42*, e13178. [CrossRef]
17. Carslaw, H.S.; Jaeger, J.C. *Conduction of Heat in Solid*; Oxford University Press: London, UK, 1959.
18. Cerbelli, S.; Garofalo, F.; Giona, M. Effective dispersion and separation resolution in continuous particle fractionation. *Microfluid Nanofluid* **2015**, *19*, 1035–1046. [CrossRef]
19. Delgado, T.; Pereira, J.A.; Baptista, P.; Casal, S.; Ramalhosa, E. Shell's influence on drying kinetics, color and volumetric shrinkage of *Castanea Sativa* Mill. fruits. *Food Res. Int.* **2014**, *55*, 426–435. [CrossRef]
20. Chayjan, R.A.; Kaveh, M. Physical parameters and kinetic modeling of fix and fluid bed drying of terebinth seeds. *J. Food Proc. Pres.* **2014**, *38*, 1307–1320. [CrossRef]
21. Ndukwu, M.C.; Simonyan, K.J.; Ndirika, V.I.O. Investigation of the structural changes of cocoa bean (with and without seed coat) during convective drying. *Int. J. Agric. Biol. Eng.* **2012**, *5*, 75–83.

22. Asoegwu, S.N.; Ohanyere, S.O.; Kanu, O.P.; Iwueke C. N. Physical properties of african oil bean seed (*pentaclerthra macrophylla*). *Agric. Eng. Int. CIGR J.* **2006**, *VIII*, FP 05 006.
23. Bird, R.B.; Stewart, E.W.; Lightfoot, E.N. *Transport Phenomena*, Revised 2nd ed.; John Wiley and Sons, Inc.: New York, NY, USA, 2006.